Thermoresponsive antifouling ultrafiltration membranes from mesophase templating

Saadat, Younes
Tabatabaei, Seyed Mostafa
Kim, Kyungtae
Foudazi, Reza

To be published in: Journal of Membrane Science

DOI to publisher's version: 10.1016/j.memsci.2023.121861

Journal Pre-proof

Thermoresponsive antifouling ultrafiltration membranes from mesophase templating

Younes Saadat, Seyed Mostafa Tabatabaei, Kyungtae Kim, Reza Foudazi

PII: S0376-7388(23)00517-3

DOI: https://doi.org/10.1016/j.memsci.2023.121861

Reference: MEMSCI 121861

To appear in: *Journal of Membrane Science*

Received Date: 20 March 2023

Revised Date: 9 June 2023

Accepted Date: 17 June 2023

Please cite this article as: Y. Saadat, S.M. Tabatabaei, K. Kim, R. Foudazi, Thermoresponsive antifouling ultrafiltration membranes from mesophase templating, *Journal of Membrane Science* (2023), doi: https://doi.org/10.1016/j.memsci.2023.121861.

Credit Author Statement

Younes Saadat: Conceptualization, Methodology, Validation, Formal analysis, Investigation, Writing - Original Draft, Writing - Review & Editing, Visualization. **Seyed Mostafa Tabatabaei:** Methodology, Validation, Formal analysis, Investigation, Writing - Review & Editing, Visualization. **Kyungtae Kim:** Formal analysis, Investigation, Resources, Writing - Review & Editing, Visualization. **Reza Foudazi:** Conceptualization, Methodology, Investigation, Resources, Writing - Review & Editing, Supervision, Project administration, Funding acquisition.

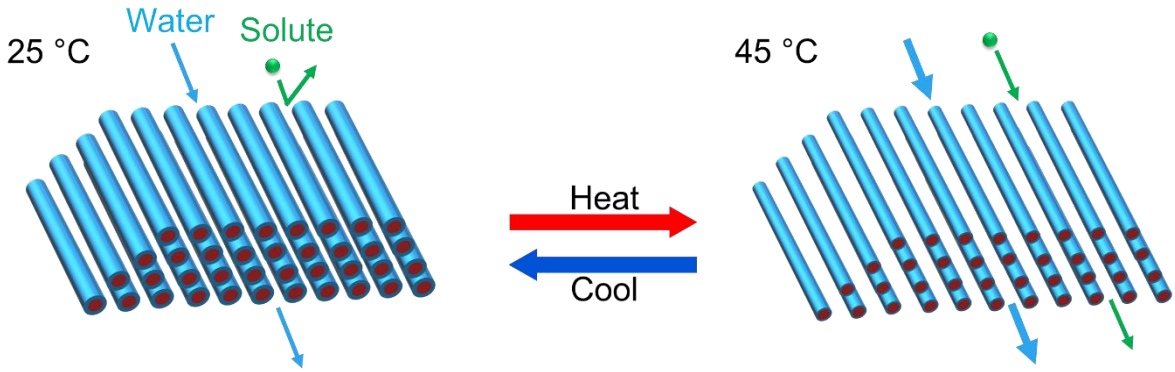

Thermoresponsive antifouling ultrafiltration membranes from mesophase templating

Younes Saadat [1], Seyed Mostafa Tabatabaei [1], Kyungtae Kim [2], Reza Foudazi [1*]

[1] *School of Chemical, Biological and Materials Engineering, The University of Oklahoma, Norman, OK 73019, USA*

[2] *Materials Physics and Applications Division, Center for Integrated Nanotechnologies, Los Alamos National Laboratory, Los Alamos, NM 87545, USA*

ABSTRACT

Nanostructured polymers synthesized by lyotropic liquid crystal (LLC) templates with normal hexagonal (H_1) structure exhibit a 3D-continuous transport path, which makes them ideal for membrane separation application. Incorporating additional functionality, especially stimuli-responsiveness, in such ordered structure provides even more application opportunities. In this work, we present the first successful synthesis of H_1-structured thermoresponsive ultrafiltration (UF) membranes via LLC templating. The membrane contains thermoresponsive Pluronic P84 diacrylate (P84DA) which not only acts as the monomer and structure-directing amphiphile, but also enables the pore size change with temperature. Experimental studies reveal that the swelling capacity of H_1-templated polymer as well as permeability and selectivity of the obtained membrane can be altered via changing the temperature. Increasing the temperature from 25 to 45 °C increases the normalized flux from 28 to 68 liters m^{-2} $hour^{-1}$ µm and molecular weight cut-off (MWCO) from 2200 to 3900 Da. Furthermore, the membrane shows an outstanding fouling resistance against different solutes.

* Corresponding author. Email: rfoudazi@ou.edu.

Keywords: *Thermoresponsive membranes, Lyotropic liquid crystals, Mesophases, Fouling resistant, Ultrafiltration, Self-assembly*

1. INTRODUCTION

Membrane separation, which can be considered as an energy-efficient and adoptable technique, is currently employed in a variety applications; e.g., treatment of different water resources [1], protein purification [2], vaccine filtration [3], food processing [4], and organic solvent filtration [5]. Despite all the offered advantages, there are still challenges involved in membrane technology. For instance, most of the membranes are only able to separate solutes with specific range of molecular sizes (i.e., fixed selectivity), resulting in their limited application [6]. Another significant challenge in membrane technology is membrane fouling, which is particularly prevalent in ultrafiltration (UF) membranes. These membranes are utilized for protein purification, food processing and removal of bacteria and viruses, which are prone to causing fouling issues [7]. Employing environmentally-questionable methods like non-solvent induced phase separation (NIPS), which consume large quantities of organic solvents to fabricate membranes in large scales, is the next notable problem in the field [8]. Creating stimuli-responsive membranes via an environmentally-friendly process can address these challenges. Such membranes can change their pore size in response to an external stimulus (e.g., temperature [6] and pH [9]), meaning that they exhibit a dynamic permeability and selectivity [10–14]. Additionally, such changes in the porosity can improve cleaning efficiency of a fouled membrane [6,15].

Synthesizing nanostructured polymers in lyotropic liquid crystal (LLC) templates (also known as LLC templating) is an environmentally-friendly approach that can be used to create such functional membranes [16–18]. As a brief background, LLCs are mesoscopic phases with a long range periodic order in the order of 2–50 nm, which form through self-assembly of amphiphiles in selective solvents [16]. Normal hexagonal (H_1) [5,17,19], normal bicontinuous cubic (Q_1) [20–23], lamellar (L_α) [15,24], and reverse hexagonal (H_2) [24] structures are the common LLC strucutres employed for synthesis of nanofiltration (NF) and UF membranes. Q_1 and H_1 phases are preferred over H_2 and L_α as they offer 3D-continuous transport path and do not require any structural alignment. In contrast to Q_1, H_1 forms more frequently and in a wider range of compositions, which makes it ideal for membrane synthesis [17]. In a recent work, Osuji and coworkers have shown the possibility of fabricating H_1-strucutred NF membranes with effective pore sizes of about 1 nm, MWCO of ~300 Da, and permeability of ~20 liters m^{-2} $hour^{-1}$ bar^{-1}, which outperform the commercially available NF membranes like Dow FILMTEC NF90-400 with a typical permeability of 10 to 15 liters m^{-2} $hour^{-1}$ bar^{-1} [19].

Despite the advantages of LLC templating, there are only a few reports available in the literature on synthesizing stimuli-responsive membranes via this technique. In one work [15], we were able to create a two-step thermoresponsive UF membrane with ~30 nm pore size from polymerization of L_α-structured LLCs directed by Pluronic F127 (F127) self-assembly, which exhibited selectivity and permeability changes at 35 and 50 °C due to the lower critical solution temperature (LCST) of F127 and melting of the crystalline structure of poly(ethylene oxide), PEO, block, respectively. Li et al. [25] reported the synthesis of a pH- and light-responsive nanoporous polymer having Q_1 structure with a pore size of around 1 nm. According to the small angle X-ray scattering (SAXS) data, the pore size changes with altering pH. While these reports on responsive membranes show

promising results, extending the pore size of LLC-templated membranes is essential to broaden their applications. In addition, there is no report on synthesizing H_1-strucutred stimuli-responsive membranes.

In this work, we report the first successful H_1-structued responsive membrane. H_1 LLC is obtained by mixing thermoresponsive Pluronic P84 diacrylate (P84DA) with 1-butyl-3-methylimidazolium tetrafluoroborate ([BMIM][BF_4]) and 1,6-hexanediol diacrylate (HDDA). Polymerized LLC (polyLLC) is acquired though UV polymerization of the mesophase. After removal of the ionic liquid with water, water transport pores are created with a pore size of 2.5 nm at 25 °C, which can be increased to 3.2 nm upon heating the polyLLC to 45 °C. Such temperature-dependent change in the porosity can increase the thickness-normalized flux of the membrane from 28 to 68 liters m^{-2} $hour^{-1}$ μm. In addition, the membrane exhibits an outstanding fouling resistance. The achieved characteristics (e.g., range of pore size, tunable selectivity, and antifouling behavior) make this membrane an ideal candidate for a variety of applications (e.g., protein purification and removal of viruses and bacteria) without having to tune the structure or change the membrane entirely.

2. EXPERIMENTAL

2.1. Materials

All of the chemicals used in this work were purchased from Sigma-Aldrich and used as received unless stated otherwise. Pluronic P84 (P84) copolymer (PEO_{19}−PPO_{43}−PEO_{19}) with an average molecular weight of 4200 g/mol, anhydrous dichloromethane (DCM) with a purity of ≥99.8%, 99.8% pure anhydrous toluene, triethylamine having a purity of 99.5% and acryloyl chloride with a purity of 97% were used to synthesize P84DA as the polymerizable surfactant (as described in the next section). [BMIM][BF_4] with a purity of ≥98%, HDDA (obtained from Thermo Scientific

Chemicals having a purity of 99%), and 99% pure 1-hydroxycyclohexyl phenyl ketone (HCPK) were used to create the desired LLC through mixing them with P84DA. Deionized (DI) water with a conductivity of 0.055 μS/cm, which was acquired from EMD Millipore Direct-Q3, was used in all experiments.

Membranes performance (e.g., MWCO, protein and dye rejection, and fouling resistance) was evaluated through filtration of different solutes including polyethylene glycol (PEG) with different molecular weights (1, 2, 3, 4, 6, 8, and 10 kDa), lyophilized powder of bovine serum albumin (BSA) with a purity of ≥96%, direct red 23 (DR23) having a dye content of 30%, and direct red 80 (DR80) with 25% dye content. CraneMat® CU463 nonwoven polyester sheet with 2 μm porosity (supplied by Neenah Filtration) was employed as a support layer for membrane fabrication. Commercially available Ultracel® regenerated cellulose membrane with a nominal MWCO of 3 kDa (which is not thermoresponsive) was purchased from MilliporeSigma and used for comparisons with thermoresponsiveness membranes synthesized in this study.

2.2. Synthesis of P84DA

P84DA was synthesized through functionalization of P84 based on a well-established procedure available in the literature [26,27]. Briefly, 40 g of P84 was dissolved in a 150 mL mixture of DCM and toluene (DCM/toluene volume ratio of 80/20) under vacuum. Then, the mixture having a total volume of 190 mL was placed in an ice water bath followed by addition of triethylamine (2.5 mL). Subsequently, 1.2 mL acryloyl chloride was dissolved in 40 mL DCM and the obtained solution was added to the reaction mixture drop-wise in around 30 min to control the heat of reaction. The reaction medium was stirred for about 24 h under a static vacuum at room temperature. The precipitated triethylammonium chloride, which is the by-product of the reaction, was separated

from the polymer solution using Büchner funnel vacuum filtration. At the next step, the functionalized polymer was precipitated in excess n-hexane having a temperature of about −18 °C. Subsequently, the obtained polymer was washed three times with n-hexane through addition of excess amount of the *n*-hexane (about twice of the volume of the polymer) and stirring at 400 rpm with magnetic stirrer for 10 min and dried under vacuum for 3 days. Attenuated total reflectance-Fourier transform infrared spectroscopy (ATR-FTIR, Nicolet™ iS50 FTIR Spectrometer) and nuclear magnetic resonance (^{1}H NMR, Varian VNMRS-400 with Probe AutoX-DB-PFG) were used to evaluate the extent of the functionalization reaction (see section S1 in supplementary information, SI).

2.3. Mesophase preparation

The H_1-structured mesophase was prepared via mixing P84DA, [BMIM][BF4] (containing 1 wt% HCPK as UV initiator), and HDDA (containing 10 wt% HCPK) with a weight ratio of P84DA/[BMIM][BF4] /HDDA 48.6/48.6/2.8. Hand mixing and centrifugation at 11,000 rpm for 5 min in a 50 mL centrifugal tube were carried out repeatedly until a transparent gel was obtained. Fig. 1 represents the chemical structure of the components used for mesophase preparation. Additionally, schematic of the created H_1 structure is presented in Fig. 1e.

2.4. Characterization of LLC and polyLLC

2.4.1. Cross-polarized light microscopy (CPLM)

A cross-polarized Nikon microscope (model LABOPHOT2-POL) equipped with a digital camera was used to evaluate the birefringence of the H_1-structured sample before and after polymerization. Around 0.2 g of the mesophase gel was sandwiched between a glass slide and a glass cover slip

for CPLM analysis. To polymerize LLC, the sandwiched sample was cured via UV radiation (using Uvitron Sunray 600 SM curing system equipped with a 600 W UV flood lamp) for 40 s. Structure of the polymerized LLC is schematically shown in Fig. 1e.

2.4.2. Small angle X-ray scattering (SAXS)

SAXS was employed to further evaluate the mesophases of different samples. LLC gel was loaded into quartz capillary tubes with a nominal diameter of 1.5 mm (Charles Supper Company, Natick, MA) and sealed with epoxy glue. The loaded mesophase was cured under UV for 40 s to obtain the polyLLC for SAXS analysis. To analyze the water-swollen sample, the polyLLC was taken out of the capillary tube via breaking it and immersed in water for at least 72 h for the solvent exchange (exchange of water with the ionic liquid) and swelling. Then, the water-swollen sample was pushed into a capillary tube followed by sealing with epoxy glue. One dimensional (1D) scattering profiles were obtained from a Bruker Nanostar X-ray scattering system equipped with a monochromatic Cu Kα radiation source (X-ray wavelength of 1.541 Å) through azimuthal integration of two-dimensional (2D) scattering patterns. SAXS analysis was also performed at different temperatures for LLC gels and water-swollen polyLLCs to assess any structural changes due to temperature alteration.

2.4.3. Differential scanning calorimetry (DSC)

Different species including pure P84DA, water-swollen polyLLC, and dried polyLLC (water-swollen polyLLC sample was dried under vacuum for at least 72 h) were analyzed by differential scanning calorimetry (DSC, Q2500, TA Instruments, New Castle, DE). About 10 mg of the desired sample was placed into an aluminum pan (PerkinElmer, Inc.) and sealed with a hermetic lid. The

thermal analysis was carried out from 0 to 60 °C (and vice versa) with 1 °C/min ramp. The cycle was repeated twice and the second cycle was used for analysis (after erasing the thermal history of the samples).

2.4.4. Swelling behavior of the polyLLC

A film of polyLLC having a thickness of 500 µm was created between two glass plates followed by photopolymerization at room temperature. The obtained film was washed several times with water and dried under vacuum, from which ca. 2 cm × 2 cm samples were cut for water uptake studies. Each sample was immersed in excess DI water maintained at the desired temperature (±0.1 °C) until reaching equilibrium swollen state. Then, the swollen samples were taken out of water followed by removing the excess water on the surface using paper towel. The swelling capacity (water uptake) was calculated using following equation by using the weight of the dry (W_0) and swollen (W_t) states:

$$Swelling\ Capacity = \frac{W_t - W_0}{W_0} \times 100 \quad (1)$$

The kinetics of thermoresponsiveness was analyzed by transferring the swollen sample from a water bath at 25 °C to one maintained at 45 °C followed by measuring the water uptake in the new environment at different times. To demonstrate the reversibility of the response, the sequential change of the environment (e.g., transferring back and forth between 25 and 45 °C water baths) was performed for several cycles and the swelling capacity was measured upon each environmental change.

At least three samples were analyzed for water uptake measurements and the average value along with standard deviation is reported.

2.4.5. Rheo-mechanical studies

A strain-controlled rheometer ARES-G2 (TA Instruments, New Castle, DE) was employed to study the rheological behavior of the LLC and the mechanical properties of the polyLLCs at different states. The mesophase gel was placed in between of 25 mm sandblasted parallel plate geometry (to minimize the wall slip, although our previous work showed that the wall slip is negligible in LLCs [28]) with 1 mm gap. The viscosity was measured by sweeping temperature from 15 to 50 °C in rotational mode under constant shear rate of 0.1 s^{-1}. To make the polymerized LLC and water-swollen polyLLC samples for rheological studies, the LLC was casted in between of two glass plates separated by 1 mm spacer plates. Then the cast gel was UV-polymerized for 40 s to obtain polyLLC sheet with 1 mm thickness. The polyLLC was then cut in circles having 25 mm diameter. The water-swollen samples were obtained through solvent exchange and swelling of the circular cut polyLLCs followed by trimming the swollen samples to fit the rheometer geometry. To analyze the acquired samples, dynamic frequency sweep test was carried out in the frequency range of 0.1 to 100 rad/s using 25 mm crosshatched geometry with 1 mm gap. The water-swollen samples were tested at 10, 25 and 45 °C. It should be mentioned that the dynamic frequency sweep test was performed in the linear viscoelastic regime (0.1% strain, confirmed from amplitude sweep tests).

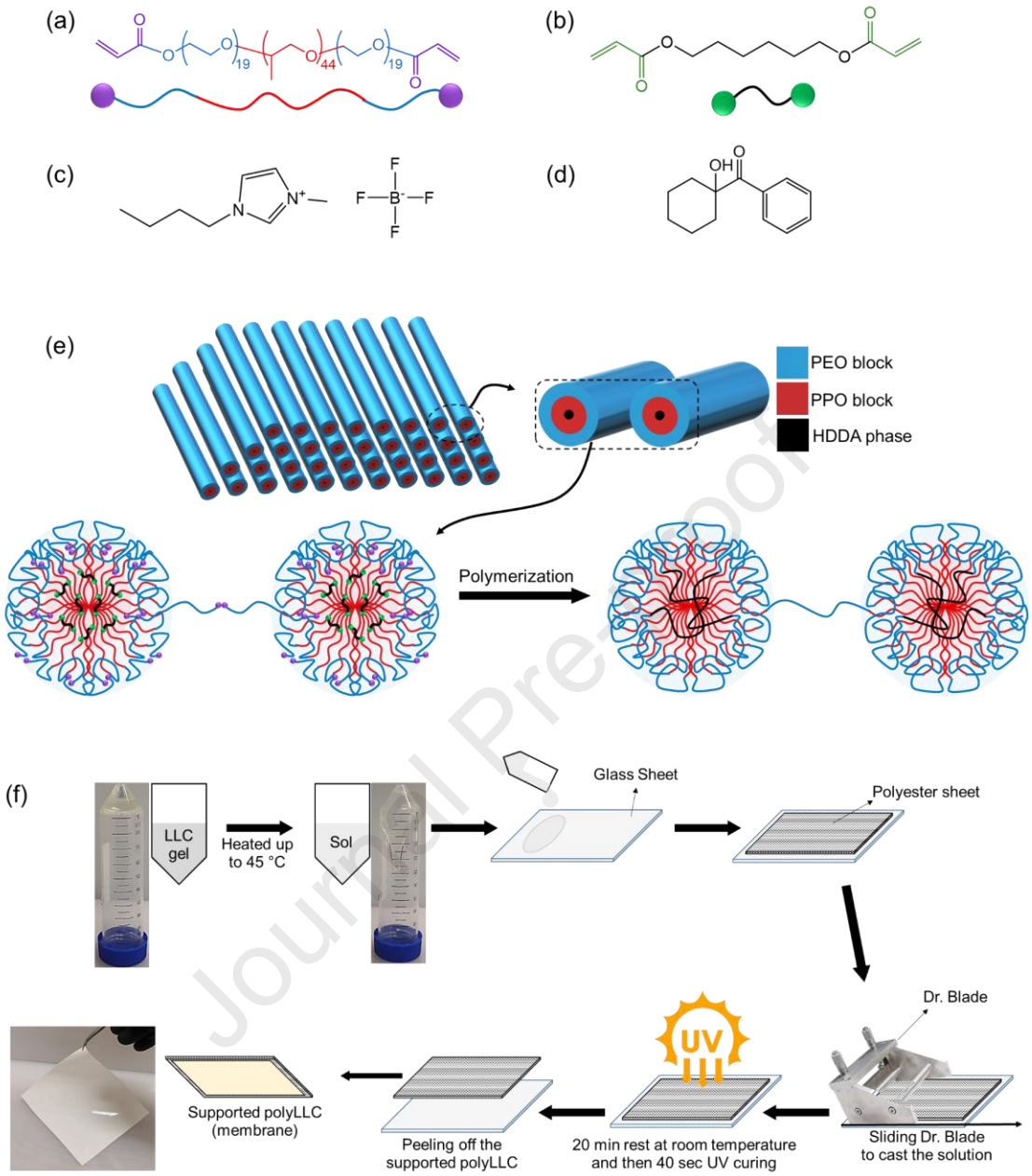

Fig. 1. Molecular structure of (a) P84DA, (b) HDDA, (c) [BMIM][BF_4] and (d) HCPK. Schematic representation of P84DA and HDDA have also been presented in panel a and b, respectively. (e) Schematic illustration of H_1-structured mesophase which is obtained through mixing the components. The micelles are surrounded by [BMIM][BF4]. The apolar domain is made of PPO block and HDDA. Chemically-bonded polymer network is created through the reaction of acrylate groups of P84DA and HDDA. The presence of intermicellar bridges, which form via the reaction of acrylate groups of extended PEO blocks, seems necessary to have an integrated H_1-structured membrane [17]. (f) Schematic procedure for preparation of polyLLC membrane.

2.5. Preparation of the polyLLC membrane

To fabricate membranes, first the mesophase was heated to 45 °C to lower its viscosity due to a reversible structural transitions (as confirmed by rheological studies, see section S2). Then, about 1.5 g of the mesophase was placed on a glass sheet followed by covering it with the polyester support layer. A doctor blade was subsequently used to coat the mesophase on the support sheet. The coated mesophase was let to equilibrate to room temperature for 20 min to recover its original H_1 structure. Finally, the LLC layer was cured via UV radiation for 40 s, resulting in the formation of the supported polyLLC membrane (Fig. 1f shows the membrane preparation procedure schematically). Scanning electron microscope (SEM, ThermoFisher Quattro S field emission environmental SEM) was used to measure the thickness of the polyLLC coated layer.

To exchange the ionic liquid with water, all of the fabricated membranes were immersed in water for at least a week before use.

2.6. Characterization of the polyLLC membrane

2.6.1. Water flux and permeability

The performance of the membranes was evaluated using Sterlitech HP4750 high pressure stirred cell (dead-end filtration system) with the effective area of 14.6 cm^2 operated under stirring at 750 rpm with a magnetic stirrer and at a pressure of 30 psi (2.07×10^5 Pa). Thickness-normalized flux (reported as liters m^{-2} $hour^{-1}$ μm) of the membranes was measured at 25 and 45 °C. To measure the flux at elevated temperature, the filtration cell containing the membrane was placed in a water bath maintained at 45 ± 1 °C. The permeate collection was started after ensuring the isothermal conditions in membrane level and having a stable flux. All of the measurements were repeated for three membranes.

Darcy's law [24] was used to calculate the membrane permeability:

$$\frac{\kappa}{l} = \frac{Q\mu}{A\Delta P} \quad (2)$$

Where Q, μ, A, ΔP, l, and κ are the flow rate, viscosity, membrane area, pressure difference across the membrane, membrane thickness, and Darcy's constant (intrinsic permeability), respectively. Thickness-normalized intrinsic permeability was calculated to cancel out the effect of thickness variation in our comparisons. Viscosity of water at 25 and 45 °C was obtained from literature [15,29].

2.6.2. MWCO, protein and dyes rejection measurements

MWCO measurements were carried out through filtration of 1 mg/mL aqueous solutions of PEG with different molecular weights (1–10 kDa). At least 5 mL of permeate was collected for each analysis. 3 mL of a reagent [30] made of potassium iodide (2 g), iodine (1.27 g), and water (100 mL) was added to 0.3 mL of the collected permeate. Then, UV-Vis spectroscopy (Thermo Scientific™ GENESYS™ UV-Vis Spectrophotometer) was used within 15 min of sample preparation to determine the concentration of the PEG in the permeate. The following equation was used to calculate PEG rejection:

$$r = (1 - \frac{C_p}{C_f}) \times 100 \quad (3)$$

In this equation, r, C_p, and C_f are rejection, solute (e.g., PEG) concentrations in the permeate, and solute concentrations in the feed, respectively. The molecular weight of the PEG that exhibits at least 90% rejection is considered as MWCO [31].

The rejection capability of the membranes for protein and dyes were studied from filtration of BSA, DR23, and DR80 dispersions in water with 1, 0.5, and 0.5 mg/mL concentration,

respectively. The concentration of the filtrated solutes in permeate was detected via UV-Vis spectroscopy. Equation 3 was used to calculate the rejection.

To assess the thermoresponsiveness of the membranes, all of the experiments were performed at 25 and 45 °C. Additionally, the experiments were repeated for three membranes and the average value along with the calculated standard deviation is reported.

2.6.3. Contact angle and fouling resistance

Contact angle of the membranes was measured by using an optical tensiometer (Biolin Scientific). Fouling resistance of the membranes was tested through filtration of aqueous dispersions of PEG with molecular weight of 10 kDa, BSA, and DR80 at 1 mg/mL concentrations. The filtration cell was filled with about 250 mL of solution at the beginning of the experiment and 5–8 mL permeate was collected every 12 h. The test was continued for 60 h and the membrane flux and rejection were recorded in 12 h time intervals.

3. RESULTS AND DISCUSSIONS

3.1. Characterization of LLC and polyLLC

Combination of CPLM and SAXS was used to confirm the structure of the LLC as well as the synthesized polyLLC at different states. As shown in Fig. 2a, CPLM confirms that the LLC is birefringent. The observed CPLM texture is the characteristic of hexagonal mesophases [32]. The birefringence remains intact after polymerization, implying that the polyLLC retains the parental structure. Furthermore, analysis of the water-swollen polyLLC at 25 °C indicates that the structure is preserved after the solvent exchange. SAXS analysis quantitatively confirms the CPLM results. As can be seen in Fig. 2d, Bragg peaks with ratios (q/q^*) of $1{:}\sqrt{3}{:}2{:}\sqrt{7}$ are detected for the

mesophase, where q is the scattering vector and q^* is the position of the principal peak in each curve. Therefore, a highly ordered H_1 structure is present in the samples. The peaks corresponding to H_1 structure (ratio of $1:\sqrt{3}$) is also seen for the polyLLC containing ionic liquid and water-swollen polyLLC. While higher peak ratios are not observed, having the characteristic birefringence of H_1 structure and the first two peaks confirm that the structure is mostly retained after polymerization and solvent exchange. Similar observation has also been reported by Forney et al. [33] and Sievens-Figueroa et al. [34] for hexagonal structures, in which some of the SAXS peaks become weak after polymerization while the synthesized polymer still exhibits some other desired characteristic peaks. This behavior has been attributed to minor changes in the structure (e.g., adhering micelles to each other [17]) after polymerization [33,34].

A variety of structural parameters including domain sizes of the synthesized polyLLC can be estimated from the SAXS data (see Fig. 3 for schematic representation of the structural parameters). The lattice parameter (a) for hexagonal structure can be calculated as [35]:

$$a = \frac{4\pi}{\sqrt{3}q^*} \tag{4}$$

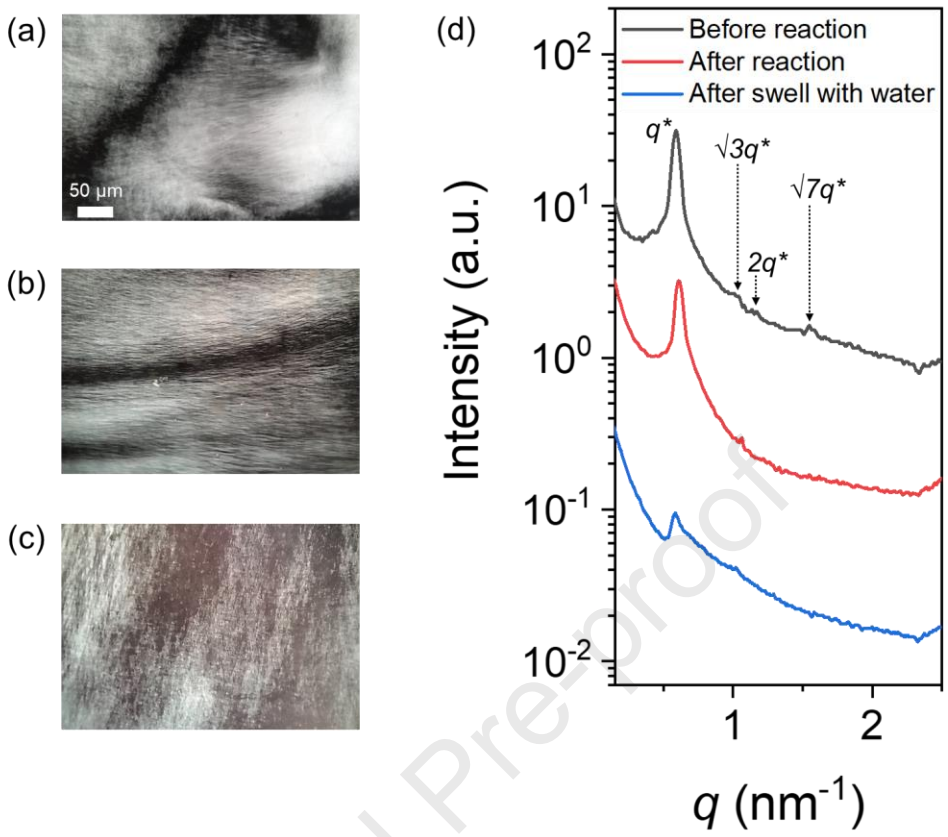

Fig. 2. (a-c) CPLM images of samples: (a) before reaction, (b) after reaction, and (c) after swelling with water. (d) 1D SAXS scattering profile for samples (the plots are vertically shifted for clarity).

To simplify the calculations, we assume that the solvent ([BMIM][BF_4] or water), PEO, PPO and HDDA are fully segregated and each domain is characterized by its bulk density [36]. It should be noted that in the case of water-swollen samples, the polymer and water are not completely segregated since the polymer network can hold large amounts of water. Another important point is partitioning the PEO and PPO blocks in the solvent and HDDA phases which makes the calculations not to be rigorously accurate [37]. The size of ionic liquid or water domain can be assumed as the pore size of polyLLC membrane. We are aware that this assumption may not be valid in all cases and that is why we have also estimated the pore size of membranes from MWCO measurements which is closer to the real application. We also assume that HDDA and PPO block

form the apolar domain with volume fraction *f*, whereas the solvent and PEO block form the polar domain that fills the rest of the volume (1−*f*). Therefore, the apolar domain size α is calculated as [35,38]:

$$\alpha = a\sqrt{\frac{\sqrt{3}}{2\pi} f} \tag{5}$$

For deriving Eq. 5, it should be noted that a hexagonal lattice with a lattice parameter of *a* has three fully occupied cylinders with a radius of α. By dividing the volume of these cylinders by the volume of a single hexagon, we can obtain the volume fraction of the cylinders (apolar domain volume fraction, *f*) as:

$$f = \frac{3\pi\alpha^2 L}{3\frac{\sqrt{3}}{2}a^2 L} \tag{6}$$

In this equation, the variable *L* represents the length of the lattice, which is equal to the length of the cylinders. By solving Eq. 6 for α, Eq. 5 is obtained.

By employing a similar approach utilized to derive the apolar domain size (α), we can define the micelle size, M_H as follows [37]:

$$M_H = a\sqrt{\frac{\sqrt{3}}{2\pi}(\varphi_{Pluronic} + \varphi_{HDDA})} \tag{7}$$

In this equation, $\varphi_{Pluronic}$ and φ_{HDDA} are the volume fraction of the block copolymer and HDDA phase, respectively. In H_1 structure after polymerization, the shortest distance between micelles is the exclusion size of solutes, which is equal to the intermicellar distance D_H [37]:

$$D_H = a - 2M_H \tag{8}$$

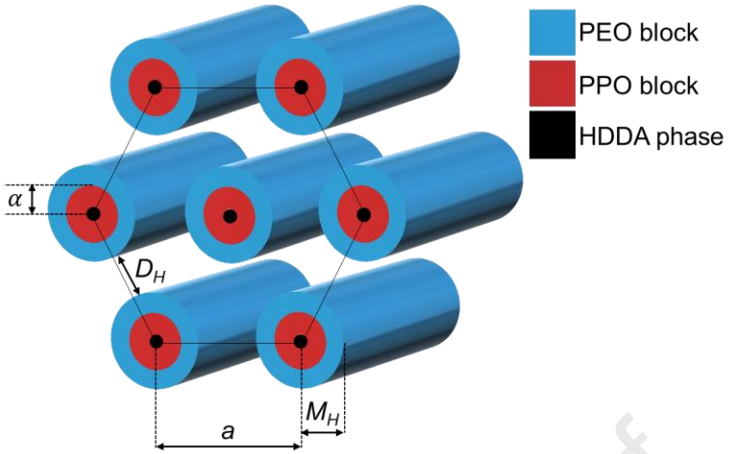

Fig. 3. Schematic representation of structural parameters for H_1 structure.

Table 1 shows the calculated structural parameters. As can be seen, the estimated intermicellar distance (pore size) is about 2.6 nm for the LLC and polyLLC. However, this estimated value significantly increases to ~5.4 nm for the water-swollen sample at 25 °C. The more accurate pore size can be determined via the MWCO experiment, which will be discussed in section 3.2.2. In the upcoming sections, we will present the experimental results of the polyLLC membrane under testing conditions of 25 and 45 °C. To enhance the comparison of the calculated data obtained from SAXS, we have also included the data for water-swollen polyLLC at 45 °C in Table 1. The corresponding SAXS data for this particular sample can be seen in Fig. 6. Section 3.2.2 will provide a detailed discussion on the calculated data.

Table 1. Calculated structural parameters for different species based on SAXS data.

Sample	q^* (nm^{-1})	φ_{PPO} [a]	φ_{HDDA}	$\varphi_{Pluronic}$	f	a (nm)	α (nm)	M_H (nm)	D_H (nm)
LLC	0.59	0.66	0.031	0.53	0.38	12.3	4.0	4.8	2.7
PolyLLC	0.60	0.66	0.031	0.53	0.38	12.1	3.9	4.7	2.6
Water-swollen polyLLC at 25 °C	0.59	0.66	0.016	0.27	0.20[b]	12.4	2.9	3.5	5.4
Water-swollen [c] polyLLC at 45 °C	0.59	0.66	0.026	0.446	0.32[b]	12.4	3.7	4.4	3.4

[a] φ_{PPO} is the volume fraction of PPO block in the Pluronic block copolymer.
[b] Volume fraction of the apolar domain for water-swollen polyLLC was calculated based on 220% and 120% swelling capacity of the polymer at 25 and 45 °C, respectively (see Fig. 5c).
[c] SAXS data for water-swollen polyLLC at 45 °C is shown in Fig. 6.

Thermoresponsiveness of the nanostructured polymer was evaluated with DSC, as shown in Fig. 4. Control experiments were also carried out on pure P84DA and dried polyLLC to define responsible phenomena for thermal transition. The water-swollen polyLLC exhibits a thermal transition in 5–32 °C range, which is attributed to the lower critical solution temperature (LCST) of Pluronic [39,40]. Hydrophilicity of the PPO block significantly decreases at LCST, reducing water solubility of the block copolymer [41]. Pure P84DA also shows a thermal transition in 20–47 °C range, which is due to the melting of crystalline regions made by PEO block [42]. In other words, since dried polyLLC has no thermal transition, we conclude that the formation of polyLLC suppresses the crystallization of PEO block and the observed thermal response of the water-swollen polyLLC is due to the LCST of the surfactant.

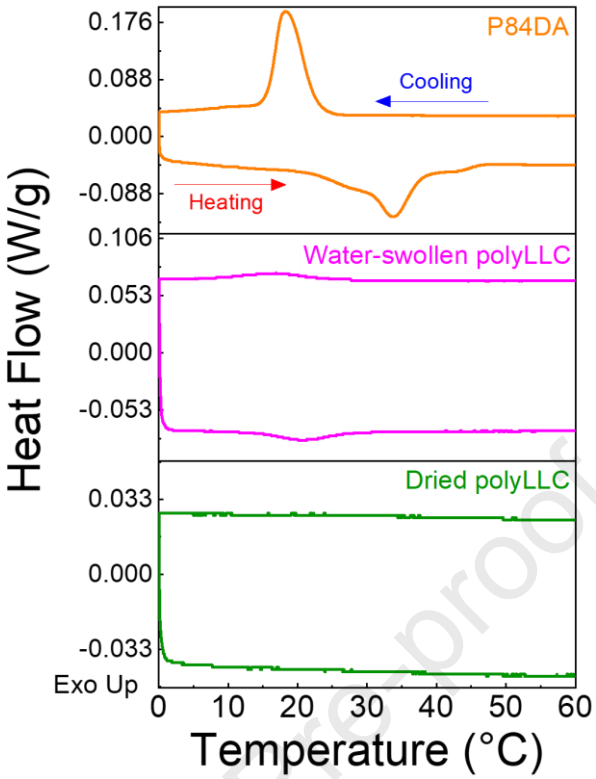

Fig. 4. DSC results for pure P84DA, water-swollen polyLLC, and dried polyLLC.

To further evaluate the thermoresponsive behavior, the swelling capacity was performed on polyLLC pieces having ca. 2 cm × 2 cm dimensions and a thickness of 500 µm (Fig. 5a–b). Fig. 5c shows that the swelling capacity of the polymer declines from ~600% to ~120% when the temperature increases from 5 to 45 °C. This change in the swelling capacity is in agreement with the DSC results, confirming that the polymer experiences an LCST transition in this range of temperature. Fig. 5d reveals that this response is rapid and takes place within 5 min. Additionally, Fig. 5e confirms the reversibility of the thermal response throughout several heating-cooling cycles.

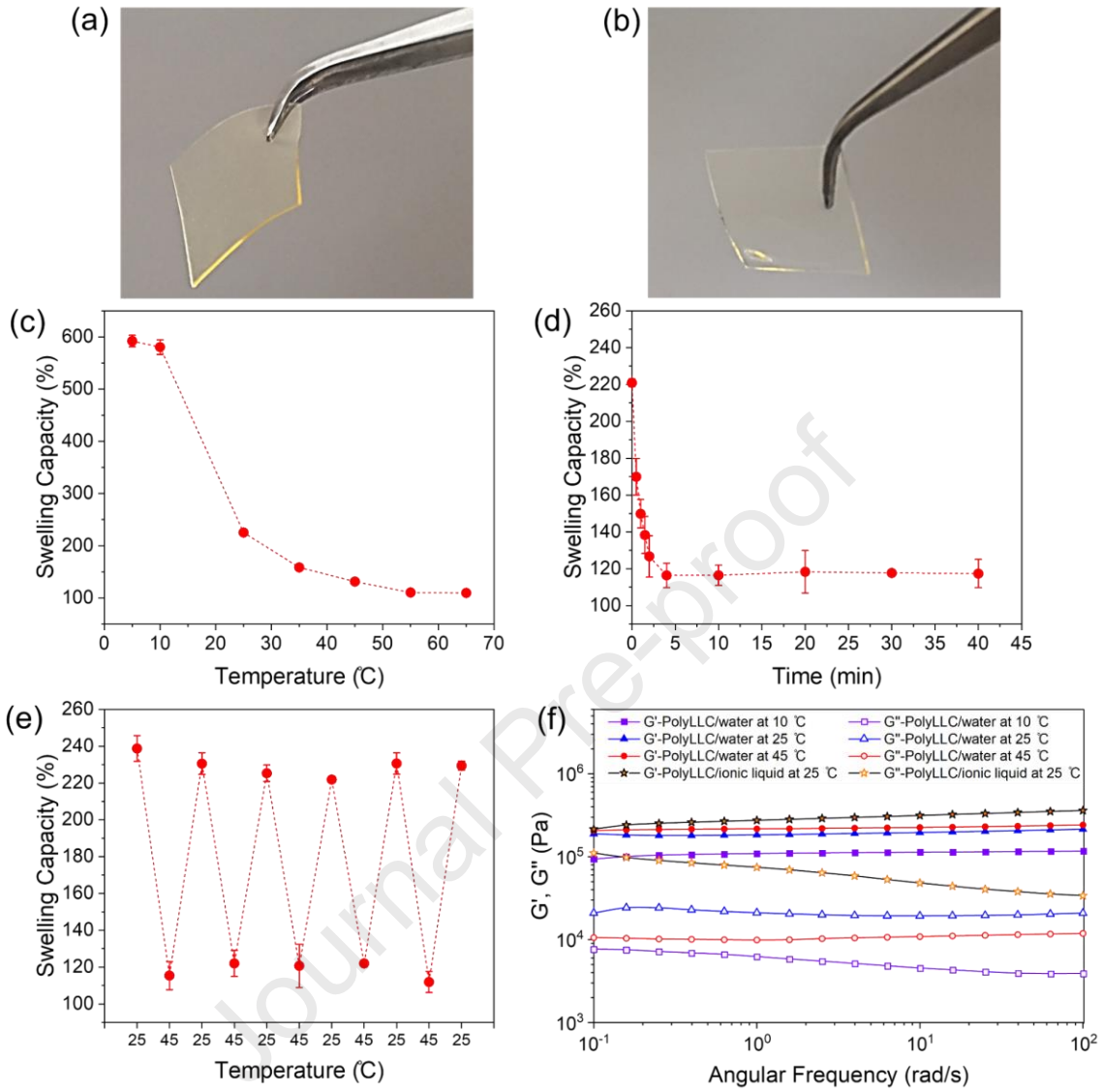

Fig. 5. (a-b) PolyLLC sample (a) before and (b) after swelling with water. (c-f) Results of different experiments: (c) swelling capacity changes with temperature; (d) kinetics of thermal response when the temperature changes from 25 to 45 °C; (e) reversibility of the thermoresponsiveness; and (f) viscoelastic behavior of polyLLC film under different conditions.

We also performed rheo-mechanical experiments on the polyLLC at different states. The results in Fig. 5f show that the polyLLC containing ionic liquid exhibits the highest mechanical strength. The storage modulus, G', of water swollen polyLLC decreases with an increase in the swelling capacity of water-swollen samples as the temperature decreases from 45 to 10 °C. These results

reveal that the mechanical properties of the obtained polyLLC is mainly affected by the solvent nature and content. In our previous study, we have shown that the elasticity of LLCs is controlled by intermicellar interactions, which change by the solvent type and intermicellar distance [43]. The solvent content at 25°C increases from 48.6 wt% in the case of polyLLC containing ionic liquid (intermicellar distance of 2.6 nm) to ~70% (intermicellar distance of 5.4 nm) after exchange of ionic liquid with water. Therefore, the higher G' for polyLLC containing ionic liquid could be attributed to the higher contents of the solvent and/or stronger intermicellar interactions. When comparing water-swollen samples, G' decreases as the solvent content (and so the intermicellar distance) increases from ~52% to ~70% and ~85 wt% by decreasing temperature from 45 °C to 25 °C and 10 °C, respectively. Similar changes in mechanical properties with variation of solvent content have been reported in the literature for solvent-swollen polyLLCs [44].

Fig. 6 shows the structural change of the water-swollen polymer with temperature, which was examined using CPLM and SAXS. The results suggest that the structure exhibits weak ordering at a temperature of 5 °C, as evidenced by the absence of texture in the CPLM image and the presence of weak peaks in the SAXS profile. As mentioned before, PPO becomes hydrophilic at temperatures below LCST of the Pluronic [15,41], which will increase the miscibility of PEO and PPO blocks with water, leading to a substantial increase in the swelling of micelles with water. This is supported by the observation of an approximately threefold increase in the swelling capacity when the polyLLC is cooled to 5 °C (see Fig. 5). Under these conditions, the segregation between the polymer chains and the water domain is disrupted. In other words, both PEO and PPO blocks will be swollen with no discernible structure. However, the structure can be restored by deswelling of the polymer through heating, due to the segregation of PEO and PPO blocks and LCST transition of PPO/water, and thanks to the presence of the chemically cross-linked polymer

network preventing complete disruption of the structure. As such, as the temperature is increased from 5 to 65 °C, the texture and strong H_1 Bragg peaks appear in CPLM and SAXS profile, respectively. The change in the structure is reversible as the scattering profiles at 25 °C before and after carrying out the heating-cooling cycle are similar. When the temperature is increased from 25 to 45 °C, the H_1 structure remains intact with lattice parameter of 12.4 nm, whereas the swelling capacity decreases from ~230% to 120%. It should be noted that the intermicellar distance of 3.4 nm can be calculated for the deswollen sample at 45 °C (see Table 1) which is in good agreement with 3.2 nm pore size obtained from MWCO measurement at 45 °C (see section 3.2.2). These results suggest that upon swelling-deswelling of the polymer network, the intermicellar distance changes due to change in the micelle size (M_H) while the overall structure remains intact (Fig. 9 schematically shows the mechanism and section 3.3 provides further discussion).

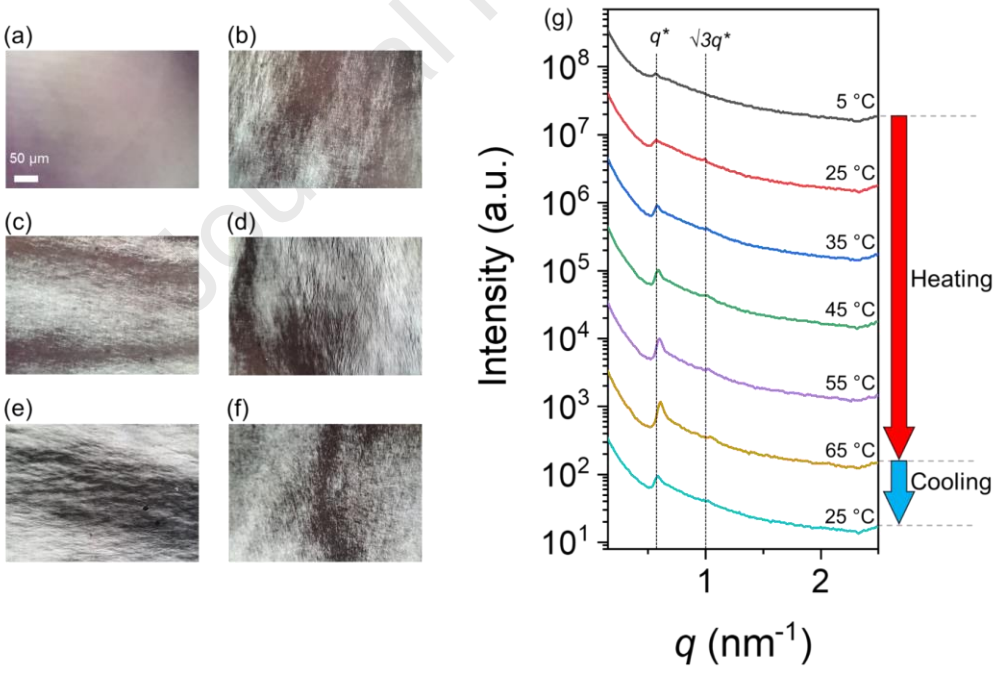

Fig. 6. (a-f) CPLM images of water-swollen polyLLC at (a) 5, (b) 25, (c) 35, (d) 45, (e) 55, and (f) 65 °C. (g) 1D SAXS scattering profile of the water-swollen polyLLC upon heating and cooling experiment. The experiment starts by heating the sample from 5 to 65 °C and ends by cooling it to 25 °C. The plots are vertically shifted for clarity.

3.2. Characterization of membranes

LLCs have gel-like behavior [28,43], which can make their casting as thin film challenging. As explained in section S2 of supplementary information, the obtained LLC exhibits H_1 structure at room temperature, which undergo a reversible structural transition upon heating. We used this behavior to lower the viscosity of the Pluronic and ionic liquid mixture for coating on a polyester sheet with doctor blade. Then, the sample was let cool down to room temperature for about 20 min, followed by UV curing for 40 s. Fig. 7a and b show a circular cut and a typical cross-sectional SEM image of the supported membrane, respectively. Image analysis revealed that the thickness of the membrane ranges 20–60 µm with an average of 40 µm. Therefore, all the membrane flux data was normalized by this average thickness to liters m^{-2} $hour^{-1}$ µm unit. We also tested a non-thermoresponsive, commercially available UF membrane as control to confirm that the observed thermoresponsive behavior is originated by the membrane (see section S3). The following sections discuss the results for polyLLC membrane performance.

3.2.1. Water flux and permeability

Water flux and permeability of the membranes were measured at 25 and 45 °C in several heating-cooling cycles. As can be seen in Fig. 7c and d, both flux and permeability increase when polyLLC membrane is heated up to 45 °C. The membrane performance returns to its original state as the temperature is decreased to 25 °C. In comparison, the commercial UF membrane does not show any changes in its permeability upon heating (Fig. S5a). These results confirm that the pore size of the polyLLC membrane can be reversibly altered by changing temperature.

3.2.2. Rejection characteristics

The MWCO experiment was first carried out at 25 °C and then at 45 °C with the same membrane. To evaluate the reversibility of the thermal response, the membrane was cooled back to 25 °C and MWCO measurement was repeated. Boltzmann sigmoidal equation was also used to fit MWCO data. The reason for employing this fitting equation is that MWCO results typically exhibit a sigmoidal trend [5].

$$y = A_2 + \frac{(A_1 - A_2)}{1 + e^{\frac{(x - x_0)}{m}}} \quad (9)$$

where A_1, A_2, x_0, and m are initial value, final value, center value, and slope at midpoint, respectively. The obtained results are shown in Fig. 7e. The MWCO is defined as the molecular weight that is 90% rejected by a membrane. The MWCO of the polyLLC membrane increases from 2200 to 3900 Da with an increase in temperature from 25 to 45 °C. The MWCO returns to 2200 Da after cooling the membrane back to 25 °C.

The membrane pore size can be estimated from MWCO by using the following equation [45]. This equation has been derived from the regression of molecular weight against the PEG hydrodynamic radius experimental data, as described by Hernández et al. [46].

$$Pore\,size = 0.12254 \times MWCO^{0.3931} \quad (10)$$

From this equation, the pore size changes from 2.5 to 3.2 nm upon heating the membrane from 25 to 45 °C. It should be noted that the estimated pore size at room temperature is in agreement with intermicellar distance from SAXS results for the as-synthesized polyLLC containing the ionic liquid. However, pore size from MWCO measurements is smaller than the intermicellar size from SAXS analysis of the water-swollen polyLLC at 25 °C. This discrepancy can be ascribed to the assumptions in our calculations based on SAXS data. In other words, the 5.4 nm pore size is

calculated from SAXS data by assuming that water and the polymer are completely segregated (water only exists within the pores). However, a large portion of water is actually trapped between the polymer chains, which is partially released upon increase in temperature from 25 to 45 °C due to change in interaction parameters of PEO and PPO blocks with water. Nevertheless, the prediction from complete segregation assumption improves at higher temperatures, as evidenced by the close correspondence between the calculated intermicellar distance of 3.4 nm from SAXS data for the deswollen sample at 45 °C (see Table 1) and the results obtained from MWCO analysis at the same temperature. This agreement suggests that at 45 °C, water primarily presents within the pores. Therefore, these results reveal that a considerable portion of water is trapped inside the polymer network (i.e., water and polymer are not segregated), which is released upon heating, resulting in the shrinkage of the polymer network and thus a larger pore size. The thermal response is perfectly reversible since the micelles are chemically cross-linked and do not disintegrate upon LCST transition.

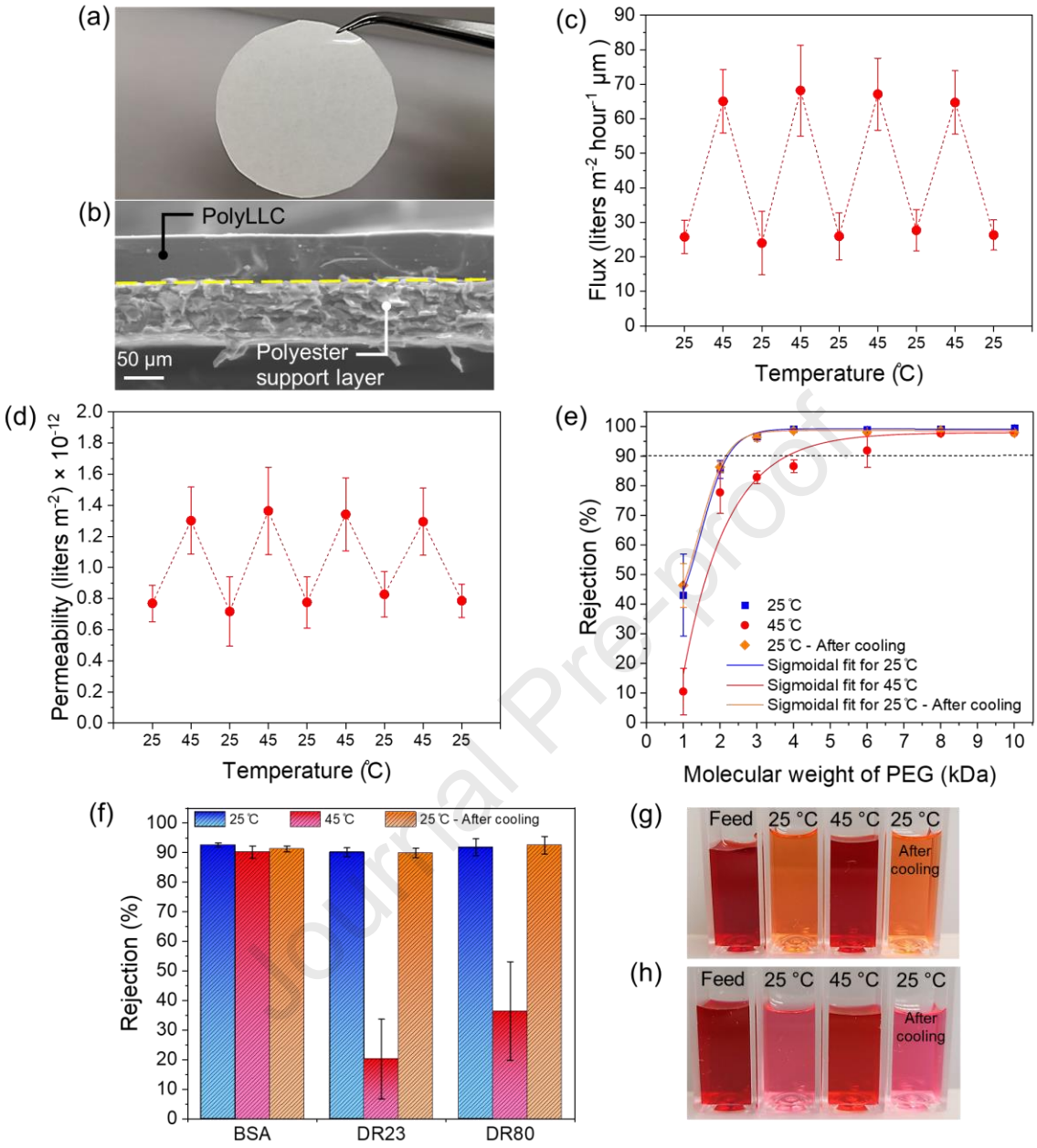

Fig. 7. (a) Circular cut supported polyLLC membrane and (b) typical cross-sectional SEM image of the membrane. (c-d) Variation of (c) thickness-normalized flux and (d) permeability with cyclic change of temperature. (e) MWCO and (f) BSA protein and red dyes rejection at 25 °C, after increasing temperature to 45 °C, and after cooling down back to 25 °C. (g-h) Photos of feed and collected permeates at different temperatures (at 25 °C, after increasing temperature to 45 °C, and after cooling down back to 25 °C) for (g) DR23 and (h) DR80.

Based on the MWCO analysis, it is observed that the pore size increases from 2.5 nm to 3.2 nm as the temperature is increased from 25 to 45 °C. Utilizing basic pore flow models such as the Hagen-

Poiseuille equation [24], this alteration in pore size can result in 2.7 times increase in membrane flux (since the flow rate is proportional to the fourth power of the pore size). Notably, this value closely corresponds to the observed 2.3 times increase in flux of our membrane when subjected to heating (see Fig. 7). The minor difference observed between the experimental data and the predicted value can be attributed to the inherent complexities, such as non-tubular pore shape and possible change of pore tortuosity after expansion of the pores upon heating.

It is worthy to mention that the commercial UF membrane having a similar pore size shows negligible changes in MWCO by increasing temperature (Fig. S5b). Furthermore, the hydrodynamic radius of PEG in the studied range of molecular weights (i.e., 1–10 KDa) exhibits negligible changes upon heating from 25 to 45 °C [47,48]. Accordingly, it can be concluded that the temperature-dependent MWCO of the polyLLC membrane is due to its thermoresponsiveness. The rejection experiment was also carried out for BSA, DR23, and DR80 at 25 and 45 °C to further study the thermoresponsiveness of the polyLLC membrane. As shown in Fig. 7f, the membrane can reject more than 90% of BSA protein. However, the rejection does not change at 45 °C. This observation is simply because of the fact that the average size of BSA molecules is ~7 nm [49], which is much larger than the membrane pore size at 45 °C.

While the membrane rejects around 90% of DR23 and DR80 at room temperature, the rejection of DR23 and DR80 significantly declines to <35% and <55%, respectively. In comparison, the commercial UF membrane does not show any changes in its rejection towards these two dyes upon heating (Fig. S5c). As it has been described in the literature [50], these dyes have a molecular size of ~1 nm, but can form clusters larger than 1 nm in water. That is why both the polyLLC and commercial membranes can efficiently reject them at 25 °C. Additionally, unlike the commercial membrane, the thermoresponsive polyLLC membrane can enlarge its pore size at 45 °C, resulting

in passage of dye clusters and thus the lower rejection rates. Fig. 7g and h show that the change in dye rejection is reversible.

We also studied the adsorption of PEG and dyes by water-swollen polyLLC to make sure that the rejection is not affected by the adsorption phenomenon. To do so, the polyLLC was added to the solutions of PEG (10 kDa molecular weight), BSA, DR23, and DR80 in such a way that the polyLLC content is 0.3 g/L (amount of polyLLC on the supported membrane in contact with the feed solution during filtration experiments). The concentration of PEG, BSA, and DR80 solutions was adjusted to 1, 1, and 0.5 mg/mL, respectively. After 48 h contact time at 25 and 45 °C, UV-Vis spectroscopy was utilized to evaluate the change in concentration of solutes. As shown in Fig S6, none of the solutes show a considerable change in concertation, meaning that the adsorption has negligible effect on the rejection performance of the membrane.

It is worth considering that we chose 45 °C temperature to test the thermal response of our membrane based on several observations. Firstly, the swelling capacity of the polyLLC changes negligibly after reaching 45 °C, as depicted in Fig. 5. Secondly, as shown in Fig. 6, there is a similar preliminary peak position in the SAXS data of the water-swollen sample at both 25 and 45 °C. Additionally, our preliminary rejection experiments with PEG molecules of 2 and 3 kDa demonstrated slight differences in the rejection rates at temperatures below 40 °C when compared to the values obtained at 25 °C. In contrast, the differences depicted in Fig. 7 were significant at 45 °C.

Lastly, it is also important to address the kinetics of the membrane thermal response, which explains the observed changes in its transport properties. Our observations indicate that the membrane performance undergoes changes at a rate comparable to the alteration in the swelling capacity of the polyLLC (see Fig. 5d) when the system reaches the isothermal conditions at 45 °C.

3.2.3. Contact angle and fouling resistance

Fouling is one of the important challenges involved in membrane separation as it can reduce the performance and thus life-time of the membrane. Fouling is more pronounced for UF membranes as they are used in pretreatment and filtration of large species (e.g., proteins, bacteria, and viruses) that cause severe fouling [1]. Increasing the surface hydrophilicity can be counted as the most important approach to limit membrane fouling [51]. Measurement of water contact angle is a simple way to examine the surface hydrophilicity of membranes [51]. Therefore, we performed this measurement on the water-swollen polyLLC membrane, and the obtained results are shown in Fig. 8a. The results present an average contact angle of 36° and 39° for the polyLLC swollen at 25 and 45 °C, respectively. This test confirms that the polyLLC membrane has highly hydrophilic surface, which can significantly enhance its fouling resistance.

To evaluate the fouling resistance, we passed the solution of three different species through the membrane maintained at 25 °C over the course of 60 h. The rejection rate was monitored in addition to the membrane flux to ensure that the reported rejection results are for steady-state conditions rather than transient state which might occur because of dead spots (fluid stagnation points) in the filtration cell, adsorption of the solute, membrane compaction, or probable leaching of materials from the system. The results presented in Fig. 8b reveal that a $\leq$6% membrane flux decline is seen after 60 h during filtration of different species. This super-fouling resistance behavior was expected as the polyLLC membrane has highly hydrophilic surface. It should also be noted that this performance is observed under dead-end filtration operation, which can induce severe fouling. Therefore, an even better performance (less than 6% flux decline) is expected under a cross-flow filtration condition. The results for the rejection of different solutes confirm that the membrane rejection performance remains almost unchanged throughout the 60 h filtration period.

It is worth noting that despite the increased hydrophobicity of the PPO block at 45 °C, the measured contact angle at this temperature only shows a negligible change compared to the value observed at 25 °C (39° versus 36°). Therefore, the alteration in the hydrophobicity of the PPO block does not significantly affect the surface hydrophilicity of the membrane, possibly due to the shielding of the PEO component. Moreover, our previous research has demonstrated that similar thermoresponsive membranes exhibit better performance against fouling at higher temperatures because pores will expand and result in a higher surface porosity when the membrane is heated up [15]. Therefore, it is not unexpected that this membrane demonstrates a similar antifouling performance at 25 and 45 °C.

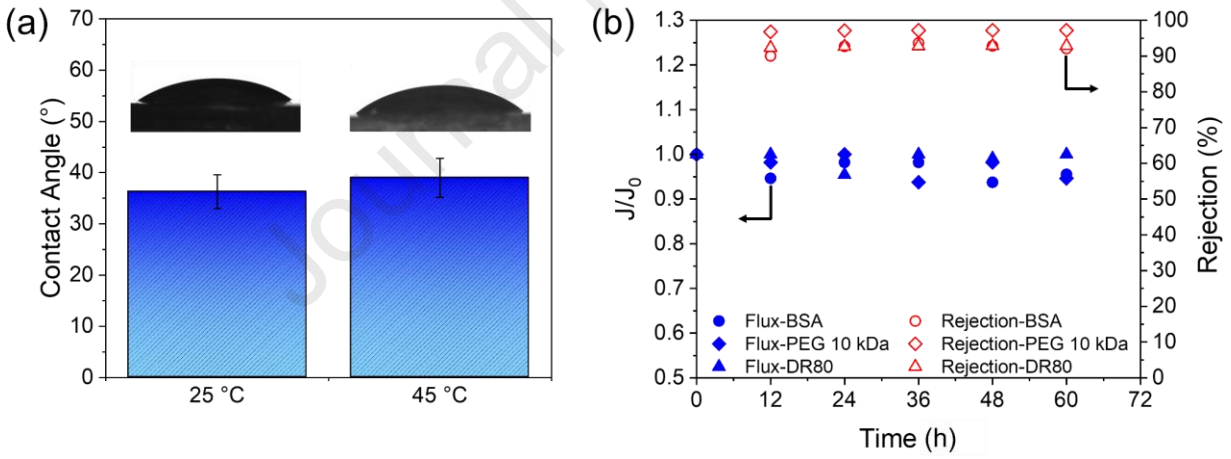

Fig. 8. (a) Contact angle of the polyLLC membrane swelled with water at 25 and 45 °C. (b) Ratio of membrane flux at a given time (J) to preliminary flux with DI water (J_0) (filled symbols) and rejection rate of different solutes (open symbols) for the polyLLC membrane.

3.3. Mechanism of thermal response

Based on the obtained experimental results, thermoresponsiveness mechanism of the polyLLC membrane can be defined as follow: a chemically cross-linked polymer network is swelled with

water, resulting in the formation of an average pores of 2.5 nm. It should be noted that due to the partial hydrophilicity of PPO block at room temperature, it is partially present in the polar domain (PEO, PPO, and water do not form fully segregated domains [52]). The PPO block in the polymer network undergoes a major dehydration upon heating to 45 °C due to the LCST of the Pluronic copolymer, resulting in the shrinkage of polymer chains. The consequent conformational change increases the intermicellar distance and result in a larger pore size (Fig. 9). This porosity alteration is perfectly reversible with rehydration of the PPO block when the system is cooled back to 25 °C. This hypothesis is in agreement with what we recently reported for the membranes synthesized via LLC templating using thermoresponsive F127 surfactant [15]. Fig. 9 represents the explained thermoresponsiveness mechanism schematically.

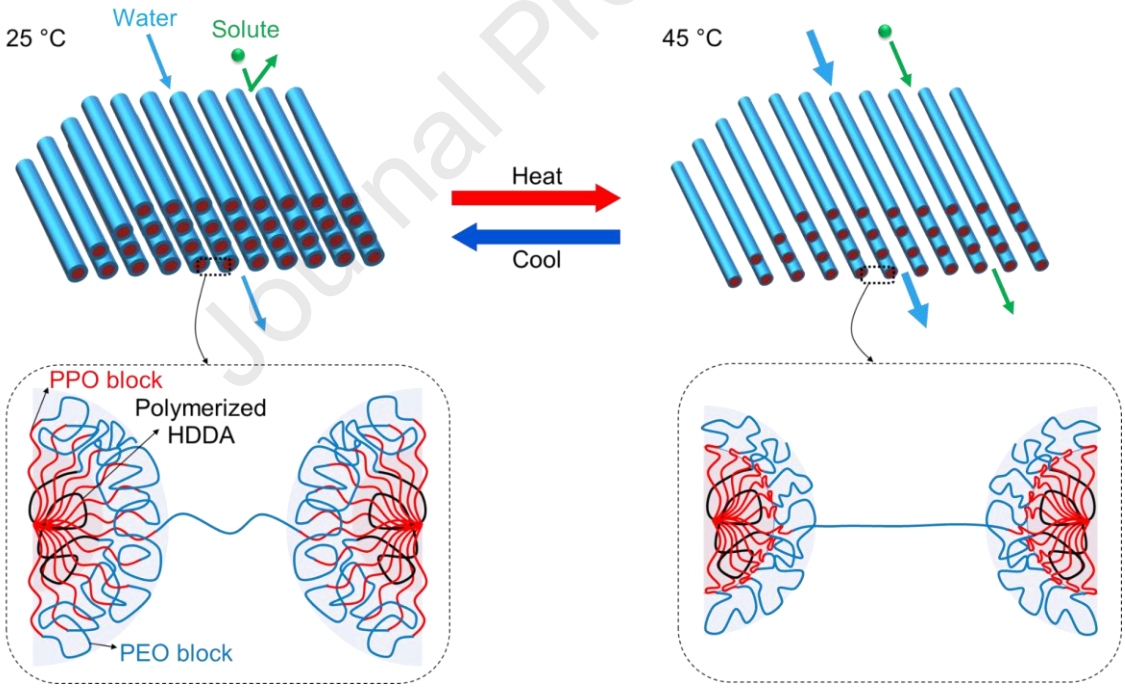

Fig. 9. Schematic representation of thermoresponsiveness mechanism of the polyLLC membrane.

4. CONCLUSION

In this paper, we reported the preparation of a mesophase-templated UF membrane with thermoresponsive and super-fouling resistant features. H_1-strucutred LLC directed by thermoresponsive P84DA block copolymer was used to synthesize the membrane. By increasing the temperature from 25 to 45 °C, the thickness-normalized flux changes from 28 to 68 liters m^{-2} $hour^{-1}$ μm and MWCO changes from 2200 to 3900 Da, respectively. Additionally, highly hydrophilic surface (contact angle of 36–39°) makes these membranes antifouling as their permeability remains almost intact after 60 h of filtration of different charged and uncharged solutes. The remarkable characteristics of this membrane render it highly suitable for a diverse range of applications. For instance, the dynamic pore size of the membrane offers the ability to finely adjust the selectivity between two components, eliminating the necessity for structural alterations or complete membrane replacement. Potential applications lie in protein purification and removal of viruses and bacteria. For protein purification or biopharmaceutical processing, however, the testing temperatures might not be raised to adjust the MWCO for separation. Nevertheless, we have shown in our previous publication that the thermoresponsive behavior can be used for cleaning membranes after fouling. The developed membrane addresses the significant fouling challenges associated with such components, irrespective of being ionic or nonionic.

ACKNOWLEDGEMENTS

The authors would like to thank the support by the National Science Foundation (NSF) under grant no. 1840871. This work was performed, in part, at the Center for Integrated Nanotechnologies, an Office of Science User Facility operated for the U.S. Department of Energy (DOE) Office of Science. Los Alamos National Laboratory, an affirmative action equal opportunity employer, is

managed by Triad National Security, LLC for the U.S. DOE's NNSA, under contract 89233218CNA000001.

CONFLICT OF INTEREST

The authors declare that they have no conflict of interest.

REFERENCES

[1] J.R. Werber, C.O. Osuji, M. Elimelech, Materials for next-generation desalination and water purification membranes, Nat. Rev. Mater. 1 (2016) 16018. https://doi.org/10.1038/natrevmats.2016.18.

[2] A. Saxena, B.P. Tripathi, M. Kumar, V.K. Shahi, Membrane-based techniques for the separation and purification of proteins: An overview, Adv. Colloid Interface Sci. 145 (2009) 1–22. https://doi.org/10.1016/j.cis.2008.07.004.

[3] F. Fallahianbijan, P. Emami, J.M. Hillsley, S.P. Motevalian, B.C. Conde, K. Reilly, A.L. Zydney, Effect of membrane pore structure on fouling behavior of glycoconjugate vaccines, J. Memb. Sci. 619 (2021) 118797. https://doi.org/10.1016/j.memsci.2020.118797.

[4] F. Salehi, Current and future applications for nanofiltration technology in the food processing, Food Bioprod. Process. 92 (2014) 161–177. https://doi.org/10.1016/j.fbp.2013.09.005.

[5] Y. Zhang, D. Kim, R. Dong, X. Feng, C.O. Osuji, Tunable organic solvent nanofiltration in self-assembled membranes at the sub–1 nm scale, Sci. Adv. 8 (2022). https://doi.org/10.1126/sciadv.abm5899.

[6] J.-Y. Choi, T. Yun, S.-Y. Kwak, Two-step thermoresponsive membrane with tunable separation properties and improved cleaning efficiency, J. Memb. Sci. 554 (2018) 117–124. https://doi.org/10.1016/j.memsci.2018.02.060.

[7] C. Güell, R.H. Davis, Membrane fouling during microfiltration of protein mixtures, J. Memb. Sci. 119 (1996) 269–284. https://doi.org/10.1016/0376-7388(96)80001-J.

[8] C. Kahrs, J. Schwellenbach, Membrane formation via non-solvent induced phase separation using sustainable solvents: A comparative study, Polymer. 186 (2020) 122071. https://doi.org/10.1016/j.polymer.2019.122071.

[9] X. Zhao, Y. Su, W. Chen, J. Peng, Z. Jiang, pH-responsive and fouling-release properties of PES ultrafiltration membranes modified by multi-functional block-like copolymers, J.

Memb. Sci. 382 (2011) 222–230. https://doi.org/10.1016/j.memsci.2011.08.014.

[10] D. Wandera, S.R. Wickramasinghe, S.M. Husson, Stimuli-responsive membranes, J. Memb. Sci. 357 (2010) 6–35. https://doi.org/10.1016/j.memsci.2010.03.046.

[11] M.K. Sinha, M.K. Purkait, Preparation of a novel thermo responsive PSF membrane, with cross linked PVCL-co-PSF copolymer for protein separation and easy cleaning, RSC Adv. 5 (2015) 22609–22619. https://doi.org/10.1039/C4RA13863E.

[12] M.K. Sinha, M.K. Purkait, Preparation and characterization of novel pegylated hydrophilic pH responsive polysulfone ultrafiltration membrane, J. Memb. Sci. (2014). https://doi.org/10.1016/j.memsci.2014.03.067.

[13] J. Fu, X. Wang, Z. Ma, H. Wenming, J. Li, Z. Wang, L. Wang, Photocatalytic ultrafiltration membranes based on visible light responsive photocatalyst: a review, Desalin. WATER Treat. 168 (2019) 42–55. https://doi.org/10.5004/dwt.2019.24403.

[14] T. Xiang, T. Lu, W.-F. Zhao, C.-S. Zhao, Ionic strength- and thermo-responsive polyethersulfone composite membranes with enhanced antifouling properties, New J. Chem. 42 (2018) 5323–5333. https://doi.org/10.1039/C8NJ00039E.

[15] Y. Saadat, K. Kim, R. Foudazi, Two-Step Thermoresponsive Ultrafiltration Membranes from Polymerization of Lyotropic Liquid Crystals, ACS Appl. Polym. Mater. 4 (2022) 8156–8165. https://doi.org/10.1021/acsapm.2c01095.

[16] Y. Saadat, O.Q. Imran, C.O. Osuji, R. Foudazi, Lyotropic liquid crystals as templates for advanced materials, J. Mater. Chem. A. 9 (2021) 21607–21658. https://doi.org/10.1039/D1TA02748D.

[17] X. Feng, Q. Imran, Y. Zhang, L. Sixdenier, X. Lu, G. Kaufman, U. Gabinet, K. Kawabata, M. Elimelech, C.O. Osuji, Precise nanofiltration in a fouling-resistant self-assembled membrane with water-continuous transport pathways, Sci. Adv. 5 (2019) eaav9308. https://doi.org/10.1126/sciadv.aav9308.

[18] E.S. Hatakeyama, B.R. Wiesenauer, C.J. Gabriel, R.D. Noble, D.L. Gin, Nanoporous, bicontinuous cubic lyotropic liquid crystal networks via polymerizable gemini ammonium surfactants, Chem. Mater. 22 (2010) 4525–4527. https://doi.org/10.1021/cm1013027.

[19] Y. Zhang, R. Dong, U.R. Gabinet, R. Poling-Skutvik, N.K. Kim, C. Lee, O.Q. Imran, X. Feng, C.O. Osuji, Rapid Fabrication by Lyotropic Self-Assembly of Thin Nanofiltration Membranes with Uniform 1 Nanometer Pores, ACS Nano. (2021) acsnano.1c00722. https://doi.org/10.1021/acsnano.1c00722.

[20] B.M. Carter, B.R. Wiesenauer, E.S. Hatakeyama, J.L. Barton, R.D. Noble, D.L. Gin, Glycerol-based bicontinuous cubic lyotropic liquid crystal monomer system for the fabrication of thin-film membranes with uniform nanopores, Chem. Mater. 24 (2012) 4005–4007. https://doi.org/10.1021/cm302027s.

[21] D.L. Gin, B.M. Carter, B.R. Wiesenauer, E.S. Hatakeyama, R.D. Noble, J.L. Barton, METHOD AND MEMBRANE FOR NANOPOROUS, BICONTINUOUS CUBIC

LYOTROPIC LIOUID CRYSTAL POLYMER MEMBRANES THAT ENABLE EACLE FILM PROCESSING AND PORE SIZE CONTROL, US 2014/0154499 A1, 2006.

[22] M. Zhou, P.R. Nemade, X. Lu, X. Zeng, E.S. Hatakeyama, R.D. Noble, D.L. Gin, New Type of Membrane Material for Water Desalination Based on a Cross-Linked Bicontinuous Cubic Lyotropic Liquid Crystal Assembly, J. Am. Chem. Soc. 129 (2007) 9574–9575. https://doi.org/10.1021/ja073067w.

[23] B.M. Carter, B.R. Wiesenauer, R.D. Noble, D.L. Gin, Thin-film composite bicontinuous cubic lyotropic liquid crystal polymer membranes: Effects of anion-exchange on water filtration performance, J. Memb. Sci. 455 (2014) 143–151. https://doi.org/10.1016/j.memsci.2013.12.056.

[24] S. Qavi, A.P. Lindsay, M.A. Firestone, R. Foudazi, Ultrafiltration membranes from polymerization of self-assembled Pluronic block copolymer mesophases, J. Memb. Sci. 580 (2019) 125–133. https://doi.org/10.1016/j.memsci.2019.02.060.

[25] P. Li, C. Johnson, S.S. Dyer, C.O. Osuji, D.L. Gin, A pH- and Light-Responsive Nanoporous Lyotropic Gyroid Polymer Network, Adv. Mater. Interfaces. (2022) 2201761. https://doi.org/10.1002/admi.202201761.

[26] C.R. López-Barrón, R. Chen, N.J. Wagner, P.J. Beltramo, Self-Assembly of Pluronic F127 Diacrylate in Ethylammonium Nitrate: Structure, Rheology, and Ionic Conductivity before and after Photo-Cross-Linking, Macromolecules. 49 (2016) 5179–5189. https://doi.org/10.1021/acs.macromol.6b00205.

[27] F. Cellesi, N. Tirelli, J.A. Hubbell, Materials for cell encapsulation via a new tandem approach combining reverse thermal gelation and covalent crosslinking, Macromol. Chem. Phys. 203 (2002) 1466–1472. https://doi.org/10.1002/1521-3935(200207)203:10/11<1466::AID-MACP1466>3.0.CO;2-P.

[28] S. Qavi, R. Foudazi, Rheological characteristics of mesophases of block copolymer solutions, Rheol. Acta. 58 (2019) 483–498. https://doi.org/10.1007/s00397-019-01162-y.

[29] J. Kestin, M. Sokolov, W.A. Wakeham, Viscosity of liquid water in the range −8 °C to 150 °C, J. Phys. Chem. Ref. Data. 7 (1978) 941–948. https://doi.org/10.1063/1.555581.

[30] J.-H. Chang, M. Ohno, K. Esumi, K. Meguro, Interaction of lodine with nonionic surfactant and polyethylene glycol in aqueous potassium lodide solution, J. Am. Oil Chem. Soc. 65 (1988) 1664–1668. https://doi.org/10.1007/BF02912573.

[31] C.J. Davey, Z.-X. Low, R.H. Wirawan, D.A. Patterson, Molecular weight cut-off determination of organic solvent nanofiltration membranes using poly(propylene glycol), J. Memb. Sci. 526 (2017) 221–228. https://doi.org/10.1016/j.memsci.2016.12.038.

[32] D.T. McCormick, K.D. Stovall, C.A. Guymon, Photopolymerization in pluronic lyotropic liquid crystals: Induced mesophase thermal stability, Macromolecules. 36 (2003) 6549–6558. https://doi.org/10.1021/ma030037e.

[33] B.S. Forney, C. Baguenard, C. Allan Guymon, Improved stimuli-response and mechanical

properties of nanostructured poly(N-isopropylacrylamide-co-dimethylsiloxane) hydrogels generated through photopolymerization in lyotropic liquid crystal templates, Soft Matter. 9 (2013) 7458–7467. https://doi.org/10.1039/c3sm50556a.

[34] L. Sievens-Figueroa, C.A. Guymon, Polymerization kinetics and nanostructure evolution of reactive lyotropic liquid crystals with different reactive group position, Macromolecules. 42 (2009) 9243–9250. https://doi.org/10.1021/ma901318f.

[35] P. Alexandridis, U. Olsson, B. Lindman, A Record Nine Different Phases (Four Cubic, Two Hexagonal, and One Lamellar Lyotropic Liquid Crystalline and Two Micellar Solutions) in a Ternary Isothermal System of an Amphiphilic Block Copolymer and Selective Solvents (Water and Oil), Langmuir. 14 (1998) 2627–2638. https://doi.org/10.1021/la971117c.

[36] P. Alexandridis, U. Olsson, B. Lindman, Self-Assembly of Amphiphilic Block Copolymers: The (EO)13(PO)30(EO)13-Water-p-Xylene System, Macromolecules. 28 (1995) 7700–7710. https://doi.org/10.1021/ma00127a016.

[37] S. Qavi, R. Foudazi, Rheological characteristics of mesophases of block copolymer solutions, Rheol. Acta. 58 (2019) 483–498. https://doi.org/10.1007/s00397-019-01162-y.

[38] P. Alexandridis, U. Olsson, B. Lindman, Phase Behavior of Amphiphilic Block Copolymers in Water−Oil Mixtures: The Pluronic 25R4−Water− p -Xylene System, J. Phys. Chem. 100 (1996) 280–288. https://doi.org/10.1021/jp951626s.

[39] E. Kushan, E. Senses, Thermoresponsive and Injectable Composite Hydrogels of Cellulose Nanocrystals and Pluronic F127, ACS Appl. Bio Mater. 4 (2021) 3507–3517. https://doi.org/10.1021/acsabm.1c00046.

[40] S. Chatterjee, P.C. Hui, C. Kan, W. Wang, Dual-responsive (pH/temperature) Pluronic F-127 hydrogel drug delivery system for textile-based transdermal therapy, Sci. Rep. 9 (2019) 11658. https://doi.org/10.1038/s41598-019-48254-6.

[41] A.M. Deliormanlı, M. Türk, Flow Behavior and Drug Release Study of Injectable Pluronic F-127 Hydrogels containing Bioactive Glass and Carbon-Based Nanopowders, J. Inorg. Organomet. Polym. Mater. 30 (2020) 1184–1196. https://doi.org/10.1007/s10904-019-01346-2.

[42] C.-F. Lee, H.-W. Tseng, P. Bahadur, L.-J. Chen, Synergistic Effect of Binary Mixed-Pluronic Systems on Temperature Dependent Self-assembly Process and Drug Solubility, Polymers (Basel). 10 (2018) 105. https://doi.org/10.3390/polym10010105.

[43] S. Qavi, M.A. Firestone, R. Foudazi, Elasticity and yielding of mesophases of block copolymers in water-oil mixtures, Soft Matter. 15 (2019) 5626–5637. https://doi.org/10.1039/c8sm02336k.

[44] J. Jennings, B. Green, T.J. Mann, C.A. Guymon, M.K. Mahanthappa, Nanoporous Polymer Networks Templated by Gemini Surfactant Lyotropic Liquid Crystals, Chem. Mater. 30 (2018) 185–196. https://doi.org/10.1021/acs.chemmater.7b04183.

[45] P.P. Marín San Román, R.P. Sijbesma, Photo-Responsive Water Filtration Membranes Based on Polymerizable Columnar Liquid Crystals with Azo Moieties, Adv. Mater. Interfaces. 9 (2022) 2200341. https://doi.org/10.1002/admi.202200341.

[46] S. Hernández, C. Porter, X. Zhang, Y. Wei, D. Bhattacharyya, Layer-by-layer assembled membranes with immobilized porins, RSC Adv. 7 (2017) 56123–56136. https://doi.org/10.1039/C7RA08737C.

[47] R. Chudoba, J. Heyda, J. Dzubiella, Temperature-Dependent Implicit-Solvent Model of Polyethylene Glycol in Aqueous Solution, J. Chem. Theory Comput. 13 (2017) 6317–6327. https://doi.org/10.1021/acs.jctc.7b00560.

[48] C. Özdemir, A. Güner, Solution thermodynamics of poly(ethylene glycol)/water systems, J. Appl. Polym. Sci. 101 (2006) 203–216. https://doi.org/10.1002/app.23191.

[49] F.L. González Flecha, V. Levi, Determination of the molecular size of BSA by fluorescence anisotropy, Biochem. Mol. Biol. Educ. 31 (2003) 319–322. https://doi.org/10.1002/bmb.2003.494031050261.

[50] J. Lin, W. Ye, M.-C. Baltaru, Y.P. Tang, N.J. Bernstein, P. Gao, S. Balta, M. Vlad, A. Volodin, A. Sotto, P. Luis, A.L. Zydney, B. Van der Bruggen, Tight ultrafiltration membranes for enhanced separation of dyes and Na2SO4 during textile wastewater treatment, J. Memb. Sci. 514 (2016) 217–228. https://doi.org/10.1016/j.memsci.2016.04.057.

[51] D. Rana, T. Matsuura, Surface Modifications for Antifouling Membranes, Chem. Rev. 110 (2010) 2448–2471. https://doi.org/10.1021/cr800208y.

[52] M. Malmsten, P. Linse, K.W. Zhang, Phase behavior of aqueous poly(ethylene oxide)/poly(propylene oxide) solutions, Macromolecules. 26 (1993) 2905–2910. https://doi.org/10.1021/ma00063a040.

Highlights

- The LLC-templated membrane shows a reversible thermoresponsive behavior
- Simple free radical polymerization chemistry is used to make the membrane
- Thermoresponsive surfactant is used to incorporate stimuli-responsiveness in the membrane
- Dynamic selectivity can be achieved by changing the temperature
- Highly hydrophilic surface of the membrane makes it fouling resistance

Declaration of interests

☒ The authors declare that they have no known competing financial interests or personal relationships that could have appeared to influence the work reported in this paper.

☐The authors declare the following financial interests/personal relationships which may be considered as potential competing interests: